

ngVLA Antenna Memo # 4

Performance of Dual-Offset Gregorian Antennas with varying Subreflector Angles

Sivasankaran Srikanth, Central Development Laboratory, Charlottesville, VA

June 18, 2019.

Abstract

The material presented in this memo is the result of analysis carried out during the optics design phase of the Next Generation Very Large Array (ngVLA) project. The major science goals for the project are described along with the chosen array configuration. Various options considered for the antenna optics are shown and the current design that is used for costing of the antenna is illustrated. This design, called the “Reference Design”, uses a dual-offset Gregorian geometry with shaped reflectors. The Reference Design antenna uses a wide-angle subreflector with an opening angle (half angle) of 55° . Performance comparison of conic section antennas with narrow-angle ($\leq 20^\circ$) and wide-angle ($\geq 25^\circ$) subreflectors are shown. Efficiency and off-axis performance have been analyzed for conic section antennas with subreflector opening angles of 41° , 46° and 55° .

1 Introduction

The initial set of science goals for the ngVLA include the study of formation of solar system analogs, probing initial conditions for planetary systems, charting the assembly, structure and evolution of galaxies, tests of gravity using pulsars in the galactic center, understanding the formation of black holes, etc. [1], [2]. The science mission translates to the requirement of an array that will have 10 times the sensitivity of the JVLA and ALMA, optimized for the 1.2 GHz to 116 GHz operating frequency range and angular resolution of 50 mas at 1.2 GHz. The main array assumes 214 x 18 m antennas, spread over baselines up to 1000 km located in greater New Mexico, eastern Arizona, west Texas and northern Mexico. An additional 19 x 6 m antennas will form a short baseline array (SBA), sensitive to a portion of the larger angular scales undetected by the main array. In mid-2018, a long baseline array (LBA) consisting of additional 30 x 18 m antennas, was included to the full ngVLA definition [3]. The array will be located at elevations over 2000m, which should allow for good observing conditions at the specified frequencies.

The specification for the antenna, calls for a design goal of 75% aperture efficiency at 30 GHz. The chosen optics for the antenna is a dual-offset Gregorian design with the subreflector/feed arm located on the lower end of the primary reflector. The reflectors are shaped for high aperture efficiency and low spillover temperature. The specification for the antenna surface error is $< 160 \mu\text{m}$ RMS that enables achieving 50% aperture efficiency at the highest receiver band [4]. The antenna design conceived currently, known as the “Reference Design”, is a low technical risk costed-concept and is the technical and cost basis of the ngVLA Astro2020 Decadal Survey proposal. The antennas will be outfitted with six receivers covering the 1.2 to 50.5 GHz and 70 to 116 GHz frequency ranges in two cryostats [5].

2 Optics Design Options

Antenna diameters ranging from 16 to 25 m were considered initially. The final size of 18 m was chosen for reasons mostly: (1) cost to meet point source sensitivity targets and (2) survey speed. Secondary factors were manufacturability/transportability and viability for supporting novel concepts that may

improve cost/performance metrics. The chosen subreflector diameter is 3.2 m, nearly the same as that of the VLBA. At 1.2 GHz, the diameter is 12.8λ resulting in diffraction loss of 7%. The subreflector diameter is 0.18x that of the main reflector and blockage loss is 7.5% on a symmetric antenna. At the least, six receivers are required in order to cover the specified frequency range (1.2 to 116 GHz). In addition to the high blockage loss in case of a symmetric antenna, locating all the receivers in the shadow of the subreflector is challenging and hence, it is necessary to gravitate towards dual-offset designs for the ngVLA antenna. This geometry comes with additional advantages like blockage-free aperture, lower sidelobes, minimized standing waves, and higher aperture efficiency. A design where the feed arm is located at the bottom of the main reflector provides easy accessibility to the receivers for servicing purposes.

Figures 1 and 2 show optics configuration for dual-offset Cassegrain and Gregorian antennas, respectively, for various (15° , 18° and 22°) subreflector opening (half) angles (θ_s). The main reflector offset distance is 9.2 m for all cases. It is to be noted that the main reflector rim-to-rim distance in the symmetric plane is larger than 18 m (19.6 m), a disadvantage of the offset geometry. Similarly, the subreflector is also larger in the symmetric plane as shown in the figures. In case of the Cassegrain antenna, the subreflector causes blockage even for the smallest subreflector angle. For the 15° antenna, a 3.8 m section of the subreflector blocks the aperture of the main reflector. The blockage can be avoided by increasing the main reflector offset distance, which will result in larger rim-to-rim distance of the main reflector. Also notice, that the subreflector size, the focal length of the hyperboloid subreflector, hence the distance of the feed from the subreflector vertex (FI) and the amount of blockage get larger with increasing subreflector angles. The Gregorian design provides a completely blockage-free aperture. The size and the focal length of the ellipsoid get smaller with increasing opening angles.

3 Reference Design for the ngVLA

The Reference Design of the ngVLA antenna uses a dual-offset reflector configuration with shaped reflectors, where $\theta_s=55^\circ$. The angle of the subreflector on AUI/NRAO/GBO centimeter wavelength radio telescopes varies between 7.2° (140-foot in Green Bank) and 15° (GBT) with the VLA at 9.3° and VLBA at 13.3° . The MeerKAT [6] antenna (13.5 m main reflector, 3.5 m subreflector) uses a much larger angle of 48.9° and the DVA-1 [7] (15 m main reflector, 3.6 m subreflector) has $\theta_s=55^\circ$. Linear taper corrugated feed horn designed to provide an illumination taper of approximately -12 dB at the edge of the subreflector, has a diameter of 15λ at the lowest frequency of operation for $\theta_s=7^\circ$, 12λ for $\theta_s=9.3^\circ$ (VLA), and 8.5λ for $\theta_s=15^\circ$ (GBT). The choice of $\theta_s=55^\circ$ for the ngVLA, allows close packing of the receivers as the feeds are smaller and the band selection mechanism viable. In order to integrate the feeds into a small number of compact dewars, quad-ridged feed horns (QRFH) [8] and axially corrugated feed horns (ACFH) [9] will be used. QRFH is smaller in size (aperture diameter of 2λ) for a given illumination taper and will be used for the lowest two bands that require about 3:1 bandwidth. The ridge profile and the horn profile are optimized for obtaining aperture efficiencies of about 70%. Wide flare angle ACFH [10] will be used for frequencies above 12.3 GHz. It has a bandwidth ratio of 2:1 and has aperture diameter of about 2λ .

Figure 3(a) shows shaped optics design currently under consideration for the ngVLA antenna. Figure 3(b) shows the conic section dual-offset Gregorian reflector design with $\theta_s=55^\circ$, from which the shaped optics was arrived. The main reflector is 18 m and the focal length of the parabola is 7.2 m. The offset distance is 9.1 m. The design in Figure 3(a) was optimized for high aperture efficiency and low spillover temperature [11]. The shape of the main reflector deviates from the parabola by +0.25 m and -1.5 m. The aperture efficiency calculated using simulated feed patterns of an ACFH (Figure 10) is about 84% at 1.8 GHz. The calculated beam pattern of the shaped system is shown in Figure 4(a). The first sidelobe is

-19.6 dB below the peak of the beam and crosspolarized sidelobe is -32 dB. A spherical wave expansion (SWE) representation of the fields of the feed horn was used in GRASP to calculate the antenna beam patterns. The beam patterns of the conic section antennas are shown in Figures 4(b) and (c) at 1.8 GHz and 17.5 GHz, respectively. The first sidelobe is -27 dB and crosspolarization is -30 dB at 1.8 GHz. Efficiency at 1.8 GHz is 65.2% and at 17.5 GHz is 67%.

4 Comparison of conic section antennas with $\theta_s = 15^\circ$, 18° and 55° at L-band

A comparison of performance of offset Gregorian antennas with subreflector angles $\theta_s = 15^\circ$, 18° (Figures 2(a), 2(b)) and 55° (Figure 3(b)) at L-band is shown in this section. For the first two cases, profile/compact corrugated horn is used, as a linear taper horn is substantially large (aperture diameter 8.51 and length 3000 mm for $\theta_s = 15^\circ$) at L-band. The profile horn is about 40% smaller in aperture and about 30% shorter compared to a linear taper horn for a given illumination taper. While a final design of the QRFH is not available at this time, for comparison purposes, this memo uses an ACFH for the 1.2 to 2.4 GHz band for the $\theta_s = 55^\circ$ antenna. Figure 5 shows the dimensions of corrugated feed horns for the three cases. The aperture diameters are 4.6λ , 3.9λ and 2.0λ at the low end of the band for the three cases of 15° , 18° and 55° , respectively. In case of the profile horns, θ_{\max} is the maximum taper angle of the inside profile and for ACFH, θ_f is the flare angle. Simulated feed patterns are shown in Figures 6, 8 and 10 for the three cases. Copolarization patterns are shown in the H- and E-planes and crosspolarization in the diagonal plane. For the profile horns, the field patterns are calculated using mode-matching technique and for the ACFH, Method of Moments technique is used. For the profile horns, the illumination taper at the edge of the subreflector does not change monotonically as a function of frequency; this is due to the fact that the phase curvature of the aperture field is the sum of that of a linear taper horn and that of an open-ended waveguide. In addition, the presence of HE_{12} mode further alters the shape of the far-field pattern. The range of the illumination taper and the average value at the edge of the subreflector are indicated in the figures. The variation of taper is substantial in case of the ACFH, particularly in the E-plane (-15.6 dB to -28.3 dB). It is to be noted that the backlobe, in case of the profile horns, is about 10 dB lower than that of the ACFH. The patterns in the principal planes are overlaid in Figures 7, 9 and 11. For the 55° horn, the symmetry of the beam deteriorates above 2.0 GHz. Figures 12 and 13 show the computed far-field patterns of the antennas at 1.8 GHz and 2.4 GHz, respectively. Beam patterns of the 15° antenna computed for a linear taper horn are also included (Figures 12(a), 13(a)). Crosspolarization at 1.8 GHz is dominated by the feed polarization for the 55° case. Computed aperture efficiency is shown in Figure 14. While difference in efficiency between the 15° and 18° cases is minor, the linear taper horn clearly results in much higher efficiency, about 10% at the center of the band. The ACFH displays about 5% lower efficiency compared to the profile horns from 1.5 to 2 GHz, deteriorates monotonically at higher frequencies and is lower by 14% at 2.4 GHz.

5 More conic section antenna designs

Analysis of antennas with subreflector angles of 55° , 46° and 41° shown in Figure 15 is covered in this section. A preliminary design of a QRFH for the $\theta_s = 55^\circ$ optics has been completed at Caltech [12]. An ACFH for the same optics has been prototyped in the 0.75-1.50 GHz band [10] and at Q-band and characterized [13]. A scaled version of the 0.75-1.50 GHz ACFH at C-band was machined at the GBO machine shop and characterized. QRFHs can be optimized to have a nominal -10 dB beamwidth in the range of 50° to 140° . A QRFH to operate at the prime focus of the GBT having an illumination taper of about -12 dB at 39° is being developed for the Ultra-wideband receiver [14]. In addition, efforts are underway in the development of QRFHs for a gamut of opening angles at several institutions. ACFHs have been developed recently at the CDL to illuminate subreflectors with $\theta_s = 46^\circ$ and 41° . These L-band designs are shown in Figures 16(b) and 16(c). The aperture diameters are 2.21 and 2.51 and θ_f is 45° and

40°, respectively. Figures 17 and 19 show simulated copolarization patterns in the H- and E-planes and crosspolarization in the diagonal plane for the two horns. The change in illumination taper in the E-plane is large compared to that in the H-plane. The change gets smaller with smaller flare angles and for the $\theta_f=40^\circ$ horn, it is 2.4 dB. Figures 18 and 20 show the circular symmetry of the beam. There is an excellent match of the patterns in the two planes for the 41° horn all the way to 2.4 GHz (Figure 20(e)).

The antenna beams at 1.8 GHz and 2.4 GHz, are shown in Figures 21 and 22, respectively. The first side lobe for the 55° antenna is marginally lower compared to the other cases at 1.8 GHz. Crosspolarization is about the same for the 55° and 41° cases and 5 dB higher compared to the 46° case in the 45°-plane. This results from the low crosspolarization of the feed horn (-35 dB) shown in Figure 18(a). At 2.4 GHz for the 55° antenna, crosspolarization is worse by 6 dB compared to the 41° antenna in the 45°-plane, caused by the feed horn polarization. Computed aperture efficiency is shown in Figure 23. Efficiency is nearly the same for the 41° and 46° antennas up to 1.7 GHz. At higher frequencies, 41° antenna has better performance, primarily because of the preservation of the circular symmetry of the feed horn pattern. The average efficiency of the 55° antenna is about 8% lower compared to the 41° antenna. This translates to a loss of 18 antennas in collecting area out of the 244 18 m antennas.

Feed dimensions and efficiencies were also calculated for the 12.5 to 21.5 GHz frequency range. As seen in Figure 24, the 41° horn is larger by 15 mm at the aperture compared to the 55° horn. Antenna beams are shown at 17.5 GHz and 21.5 GHz, in Figures 25 and 26, respectively. Crosspolarization, which is maximum in the asymmetric plane of a dual-offset antenna, is very low (<-50 dB) at these frequencies. The level of crosspolarization in the 45°-plane is about -30 dB and is caused by the feed polarization characteristics. Aperture efficiency is graphed in Figure 27, where the efficiency for a 15° antenna fed by a linear taper horn (200 mm diameter and 290 mm long) is also included. The efficiency variation for the three cases is very similar to that L-band and the loss in collecting area is equivalent to 17 antennas going from 55° to 41° optics.

A brief analysis of the scanning properties of the three antennas was carried out. The feed was displaced by 2.5 cms, 5 cms and 7.5 cms from the focus in the asymmetric plane of the antenna for the three cases and aperture efficiency was calculated for Band 3. The displacement of 2.5 cms is equivalent to 1λ at 12.5 GHz. Figure 28 shows the aperture efficiency for the three displacement cases. Here the efficiency is normalized with respect to the on-axis efficiency. For a displacement of 5 cms, efficiency decreases by 3%, 7% and 15% with respect to on-axis efficiency for the antennas with $\theta_s=41^\circ$, 46° and 55° respectively, at 17.5 GHz.

6 Conclusions

All calculations of the antenna beam patterns and efficiencies shown in the memo were carried out using TICRA-GRASP software, which is industry standard for reflector antenna analysis. The accuracy of the simulations is further enhanced, resulting from the use of SWE coefficients for representing the fields at the subreflector. Small angle subreflector ($\theta_s \leq 20^\circ$) antennas have at least 5% higher aperture efficiency at L-band compared to the 55° subreflector antenna. This is purely academic as the feed at L-band is very large for the small angle design on an 18m antenna. However, if the low end of the ngVLA frequency band is limited to 8 GHz, small angle optics using narrow flare angle linear taper feed horn becomes an option. This can increase the effective collecting area by about 15%.

Performance of antennas with subreflector angles of 41°, 45°, and 55° using ACFHs are compared at L- and Ku-bands. The 41° antenna with an ACFH of 2.5λ diameter has about 8% higher aperture efficiency compared to the 55° antenna using a 2λ diameter feed horn. The electromagnetic consulting contractors

on the project are of the opinion that the shaping of the reflectors can be optimized to yield aperture efficiency of over 80%, irrespective of the subreflector angle. It is shown that scan loss is only 3% for the 41° antenna, compared to 15% for the 55° antenna for a feed offset of 2λ . This necessitates very accurate deployment of the high frequency receivers with respect to the secondary focus in case of the 55° antenna. Shaped reflector systems display poorer scanning performance in general [15]. The dependency of scan loss on subreflector angle on shaped reflector systems has not been analyzed at present. The author suggests that scan loss for a gamut of subreflector angles on shaped reflectors be studied before the final design for the ngVLA antenna is chosen. It is very likely that spillover temperature for the three wide-angle optics covered in Section 5 is very similar, a topic beyond the scope of this memo.

Beamwidth of the QRFH varies by a larger amount compared to that of the ACFH, even over 2:1 bandwidth. Giving up continuous coverage of the 1.2 to 12.3 GHz range and using ACFH in place of the QRFH, to cover the range in two narrower bands (2:1) will result in more sensitive receivers.

The author acknowledges the comments and edits suggested by E. Murphy, M. Pospieszalski, R. Salina and P. Ward.

References

- [1] C. L. Carilli et.al. “Science Working Groups Project Overview,” ngVLA Memo # 5.
- [2] ngvla.nrao.edu/page/science
- [3] ngvla.nrao.edu/page/array-config
- [4] R. Selina and E. Murphy, “ngVLA Reference Design Development & Performance Estimates,” ngVLA Memo # 17.
- [5] W. Grammer et al., “ngVLA Front End Reference Design Description,” Document # 020.30.03.01.00-0003-DSN.
- [6] I. P. Theron, R. Lehmensiek and D. I. L. de Villiers, “The design of the MeerKAT dish optics,” European Microwave Conference.
- [7] G. Cortes, W. Imbriale and L. Baker, “DVA-1 Optics Design and Analysis,” DVA1_CDR_Optics_V3_2012_06_17.
- [8] Weinreb, S. and Mani, H., “Low Cost 1.2 to 116 GHz Receiver System – a Benchmark for ngVLA,” ngVLA Science Workshop presentation, June 2017.
- [9] R. Lehmensiek and D. I. L. de Villiers, “Wide Flare Angle Axially Corrugated Conical Horn Design for a Classical Offset Dual-Reflector Antenna,” 6th European Conference on Antennas and Propagation.
- [10] L. Baker and B. Veidt, “DVA-1 Performance with an Octave Horn; From CST & GRASP Simulations,” 2014.
- [11] L. Baker, “Analysis of ngVLA Design #6 With Ideal and Actual Feed,” Document #: 020.25.01.00.00-0001-REP ngVLA Optical Reference Design, January 2017.
- [12] J. Shi, S. Weinreb, W. Zhong and X. Yin, “Quadruple-Ridged Flared Horn Operating from 8 to 50 GHz,” Internal Memo, Dept. of Electrical Engineering, California Institute of Technology, Pasadena, CA, December 1, 2016.
- [13] L. Locke, L. B. G. Knee, F. Jiang, V. Reshetov and L. Baker, “ngVLA Communities Studies Report: Feed and Receiver Development at NRC, Herzberg,” ngVLA Memo #32.
- [14] S. White, GBO, Private communication.
- [15] P. J. Napier, “Beam Scan Properties of Non-parabolic Reflectors,” NLSRT Memo No. 46, Jan 14, 1989, NRAO, Socorro, NM.

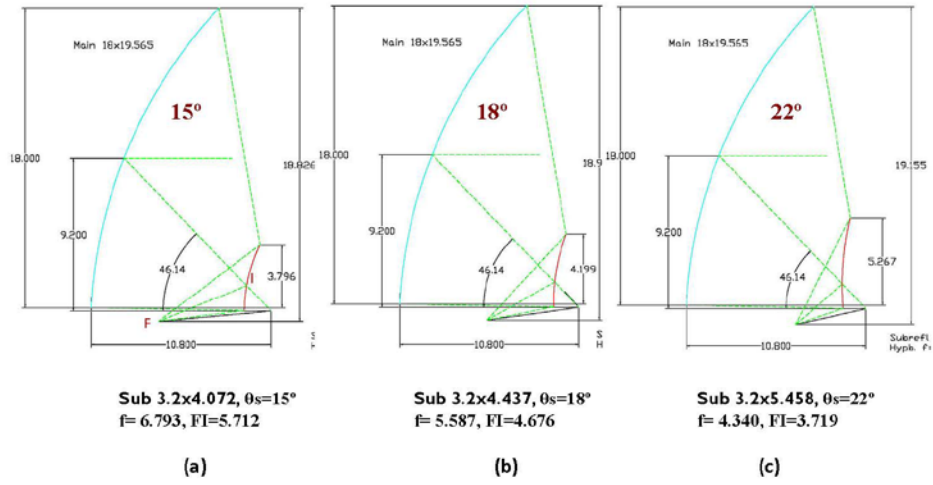


Figure 1. Dual-Offset Cassegrain antenna with $\theta_s = 15^\circ, 18^\circ, 22^\circ$.

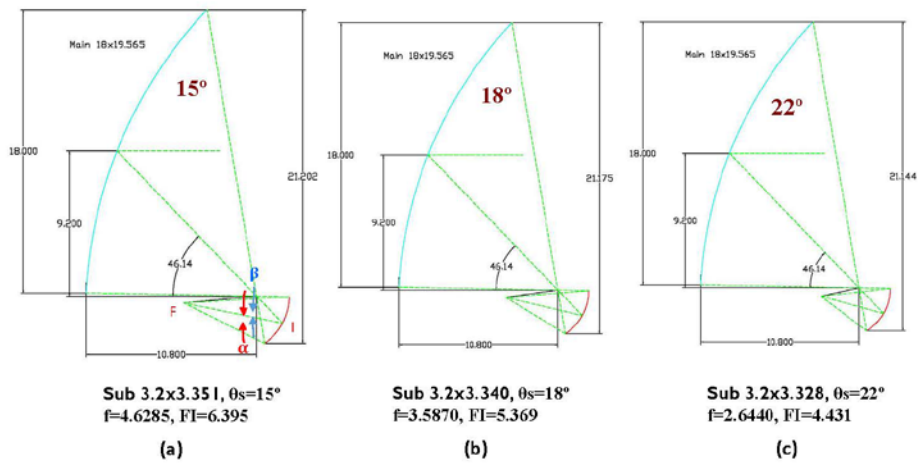


Figure 2. Dual-Offset Gregorian antenna with $\theta_s = 15^\circ, 18^\circ, 22^\circ$.

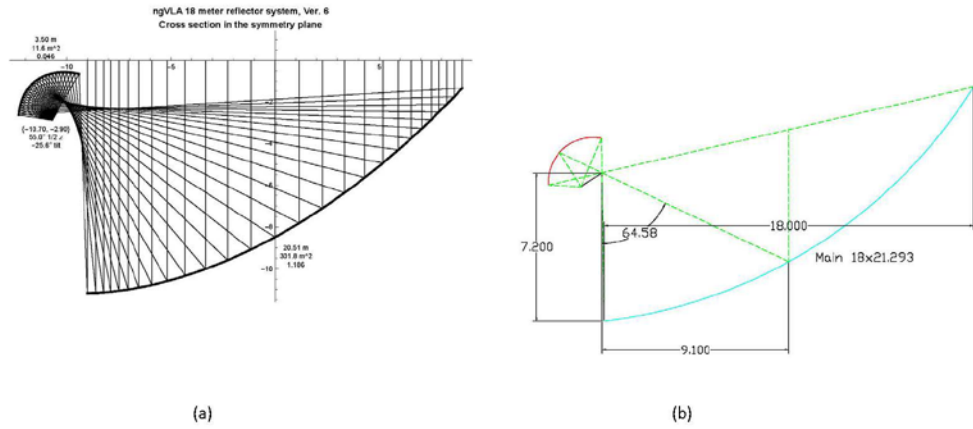


Figure 3. (a) Reference Design shaped antenna, (b) Conic section antenna.

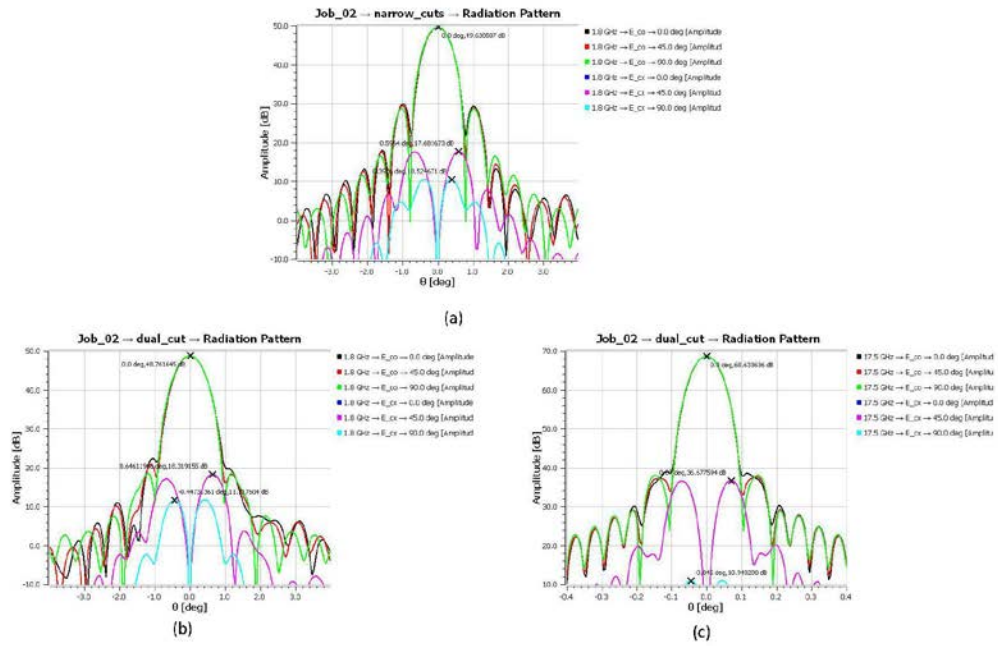


Figure 4. (a) Shaped antenna beam at 1.8 GHz, (b) Conic section antenna beam at 1.8 GHz, (c) Conic section antenna beam at 17.5 GHz.

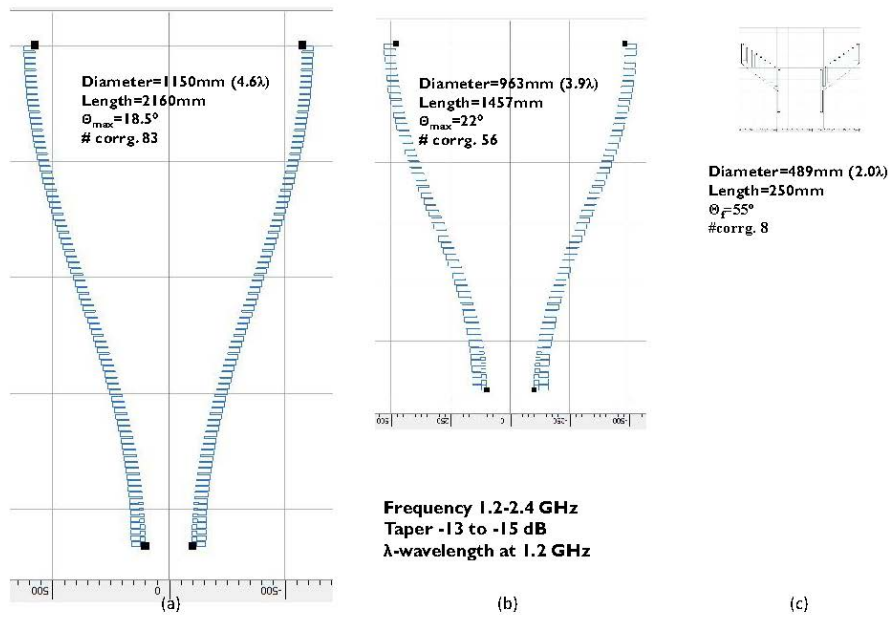


Figure 5. (a) Profile Feed Horn $\theta_s=15^\circ$, (b) Profile Feed Horn $\theta_s=18^\circ$,
 (c) Axially Corrugated Feed Horn $\theta_s=55^\circ$.

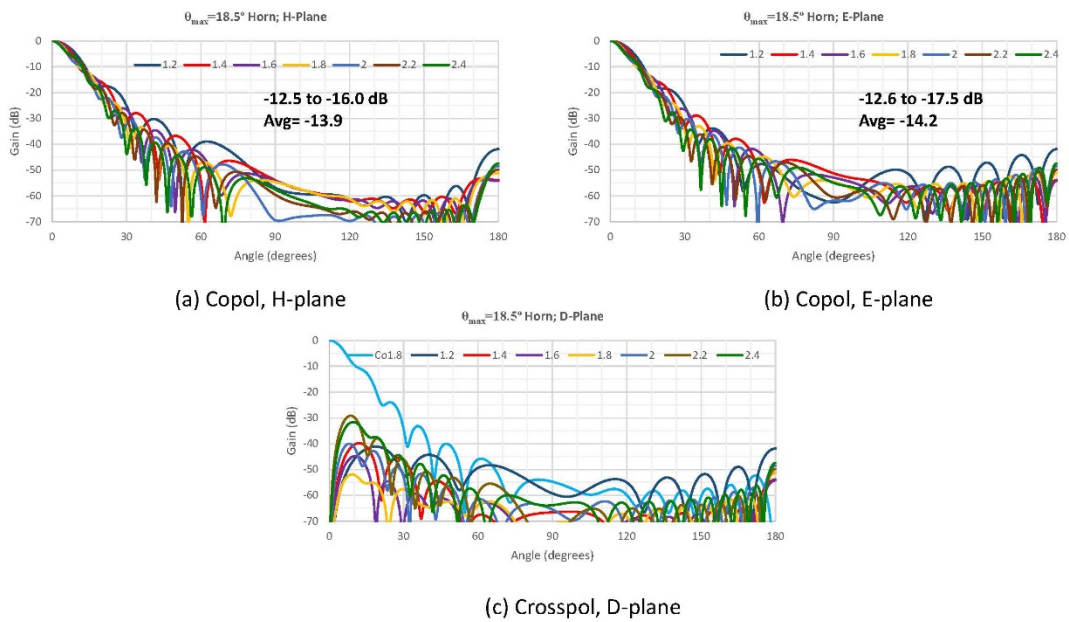


Figure 6. Simulated Copolar, Crosspolar Patterns of Profile Horn for $\theta_s=15^\circ$.

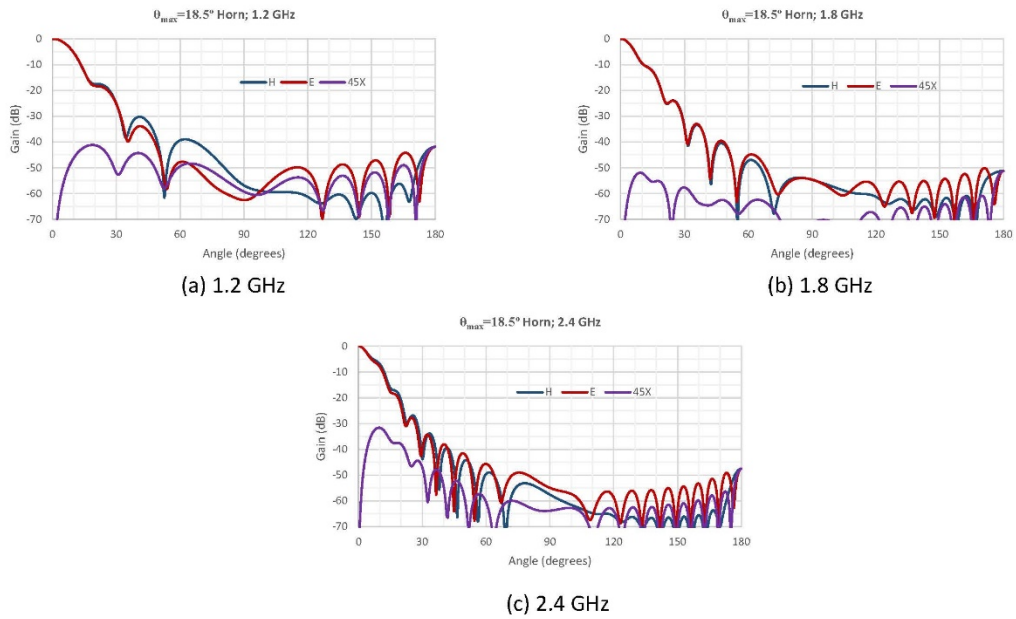


Figure 7. Simulated Copolar (H, E-planes), Crosspolar (D-plane) Patterns of Profile Horn for $\theta_s = 15^\circ$.

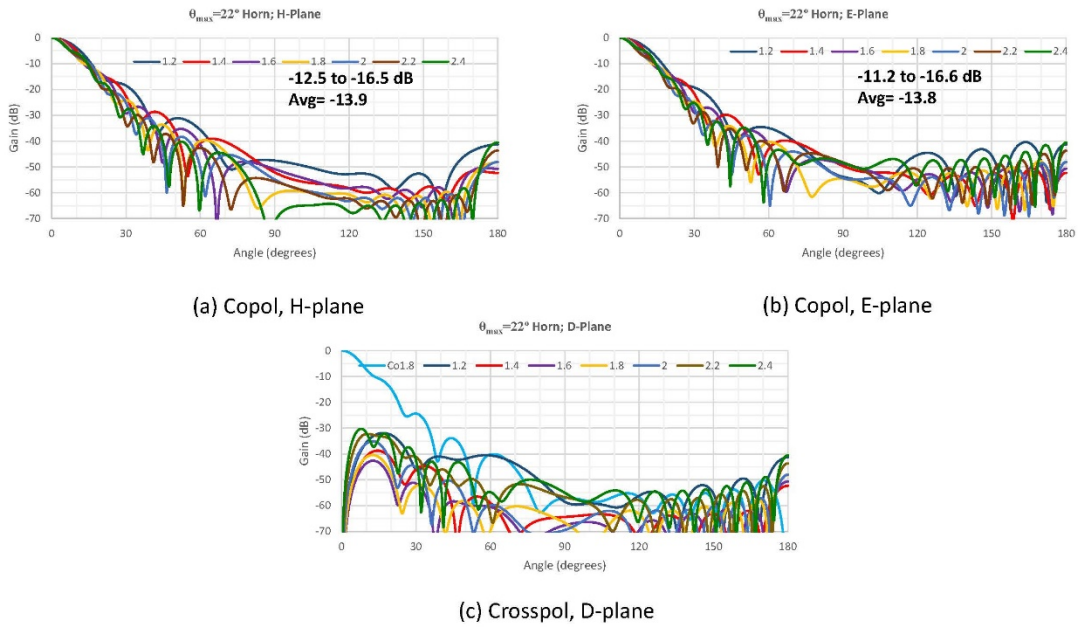


Figure 8. Simulated Copolar, Crosspolar Patterns of Profile Horn for $\theta_s = 18^\circ$.

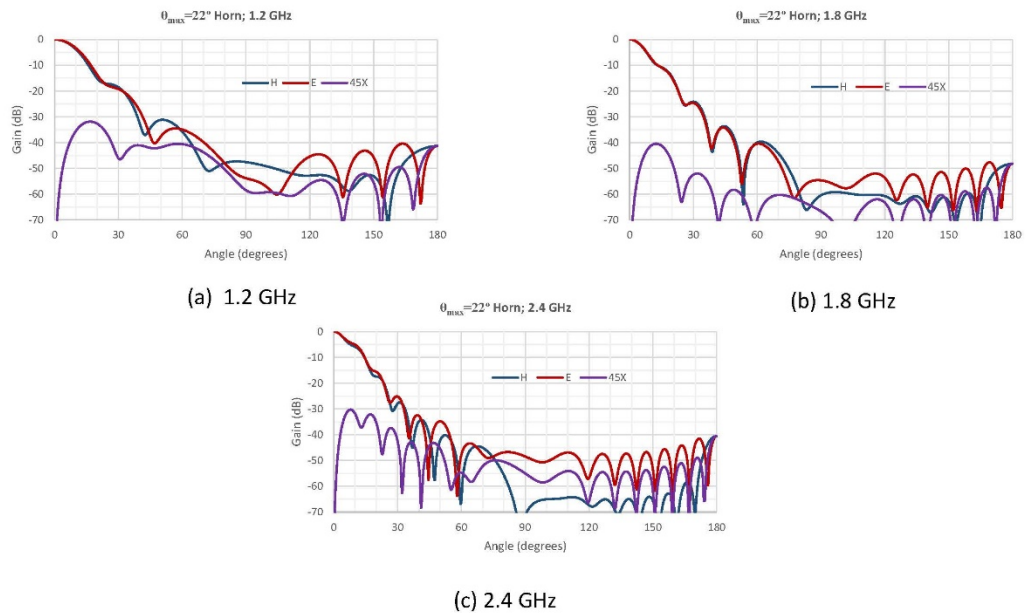


Figure 9. Simulated Copolar (H, E-planes), Crosspolar (D-plane) Patterns of Profile Horn for $\theta_s = 18^\circ$.

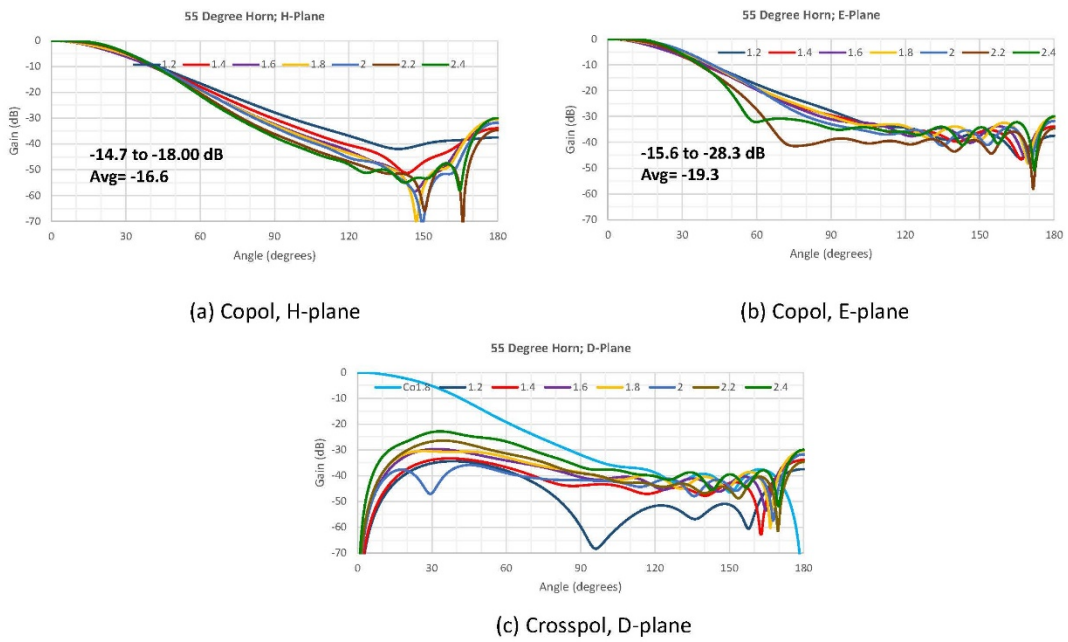


Figure 10. Simulated Copolar, Crosspolar Patterns of ACFH for $\theta_s = 55^\circ$.

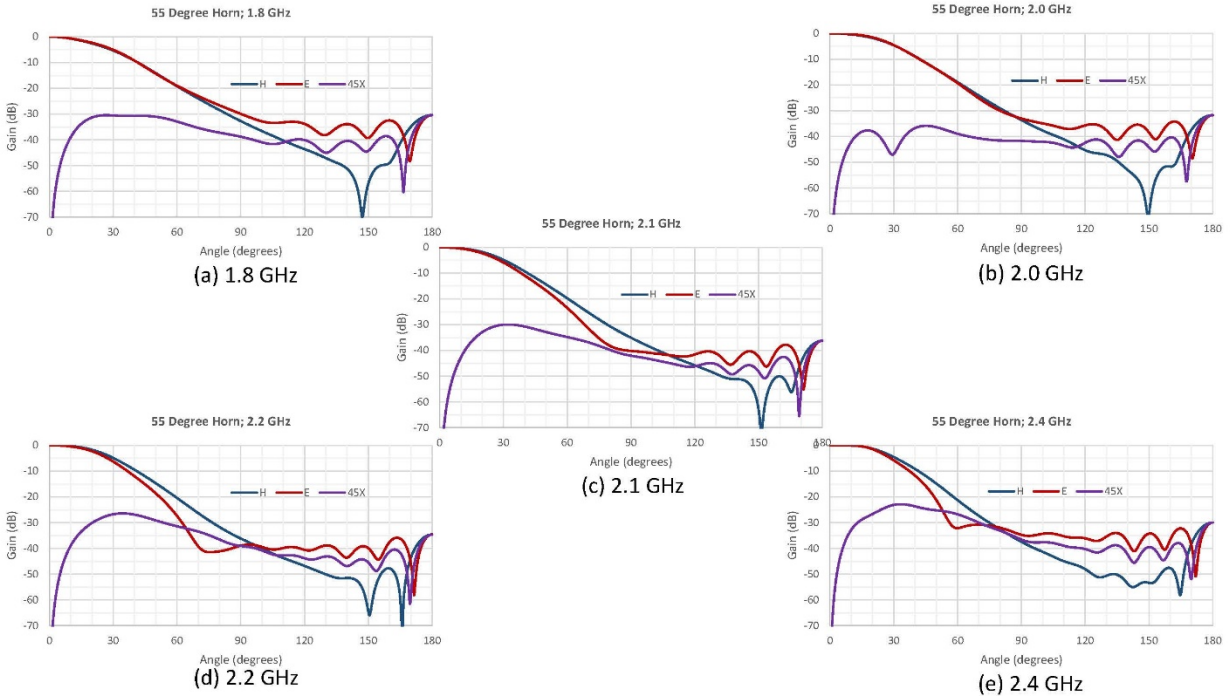


Figure 11. Simulated Copolar (H, E-planes), Crosspolar (D-plane) Patterns of ACFH for $\theta_s=55^\circ$.

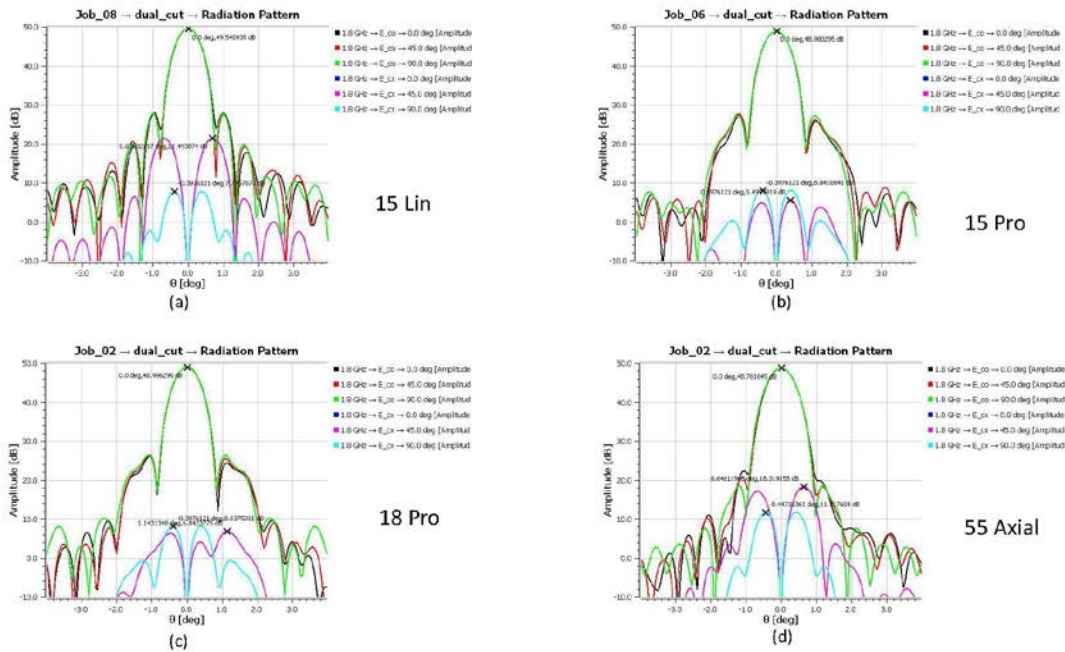


Figure 12. Antenna Beam at 1.8 GHz, (a) Linear $\theta_s=15^\circ$, (b) Profile $\theta_s=15^\circ$, (c) Profile $\theta_s=18^\circ$, (d) ACFH $\theta_s=55^\circ$.

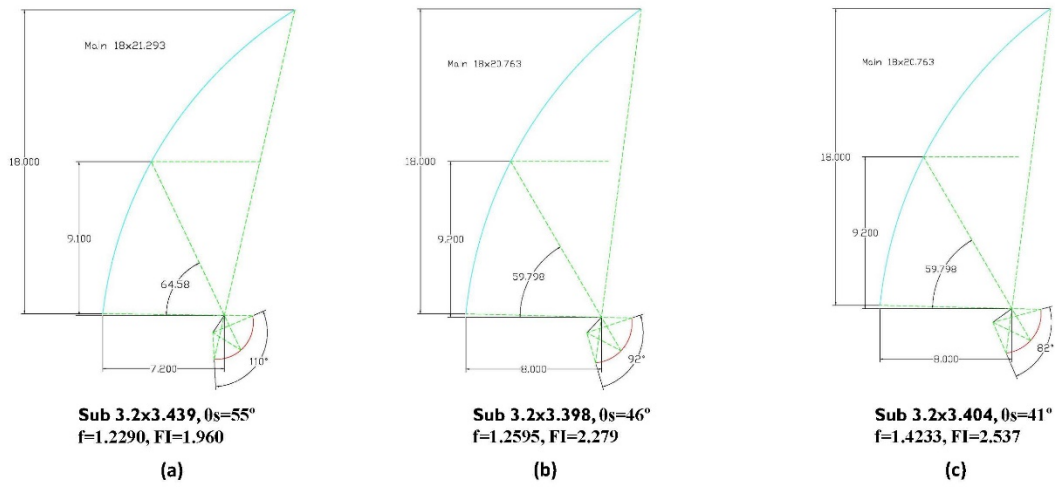


Figure 15. Dual-Offset Gregorian antenna with $\theta_s = 55^\circ, 46^\circ, 41^\circ$.

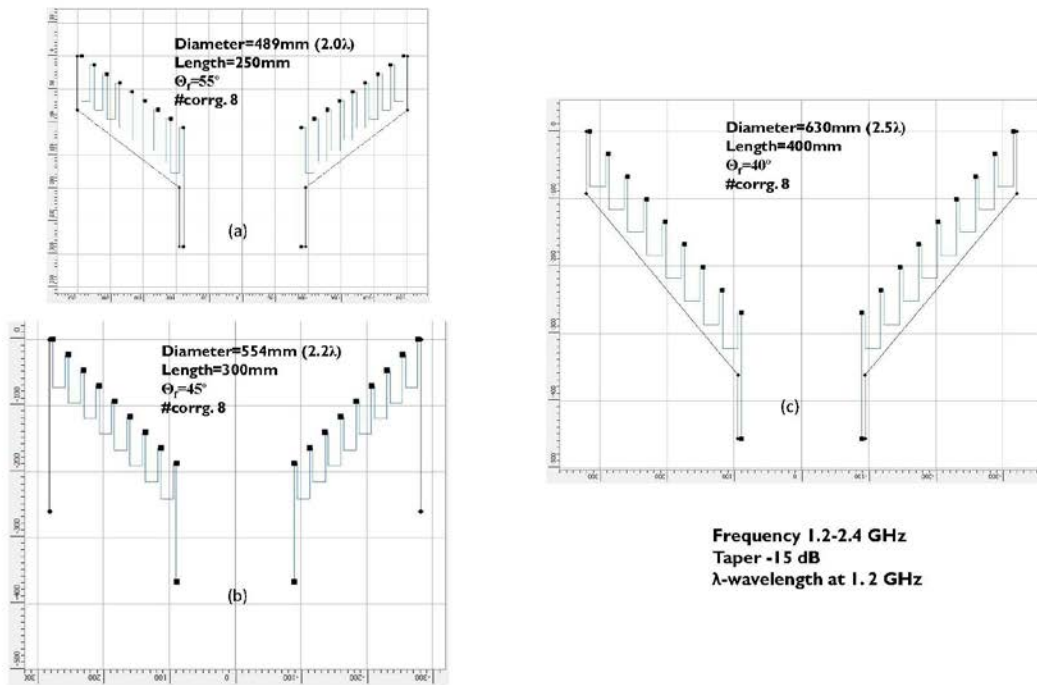
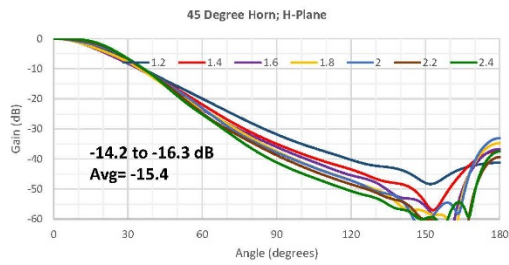
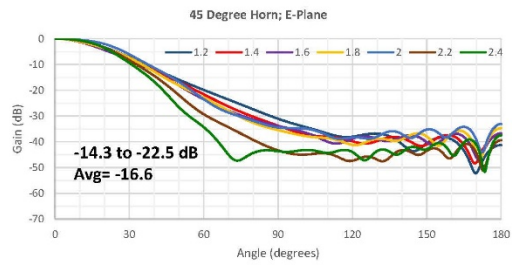


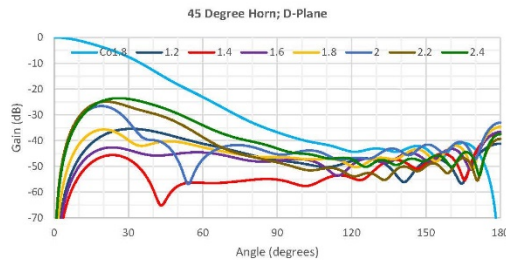
Figure 16. Axially Corrugated Feed Horn (1.2 – 2.4 GHz) for (a) $\theta_s=55^\circ$, (b) $\theta_s=46^\circ$, (c) $\theta_s=41^\circ$.



(a) Copol, H-plane

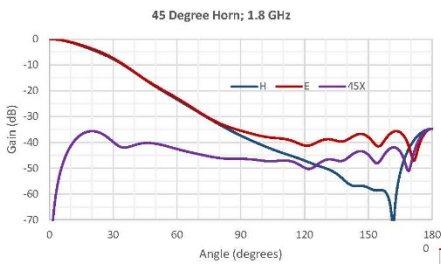


(b) Copol, E-plane

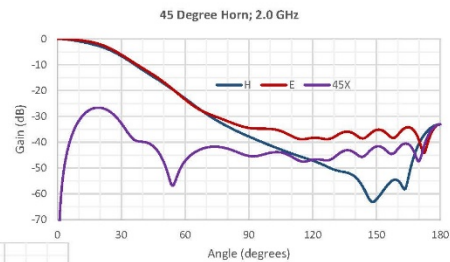


(c) Crosspol, D-plane

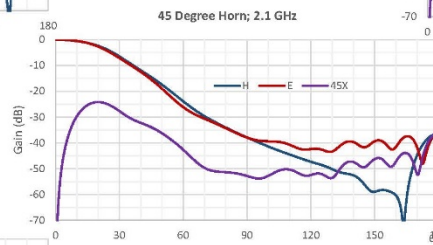
Figure 17. Simulated Copolar, Crosspolar Patterns of ACFH for $\theta_s=46^\circ$.



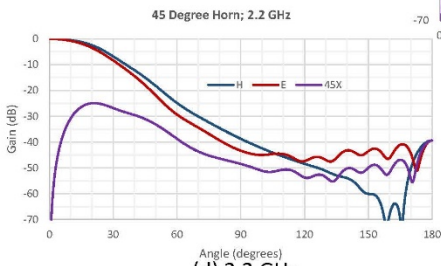
(a) 1.8 GHz



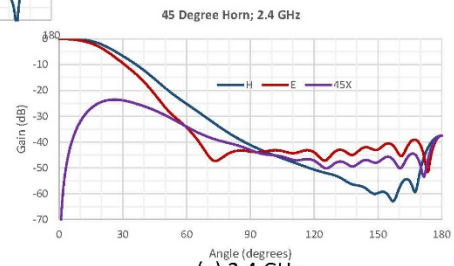
(b) 2.0 GHz



(c) 2.1 GHz

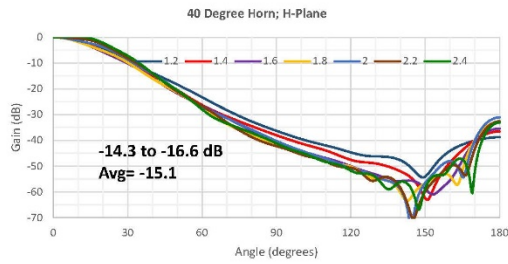


(d) 2.2 GHz

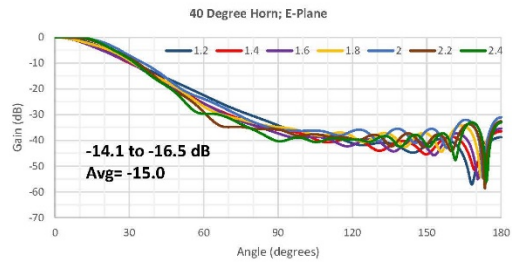


(e) 2.4 GHz

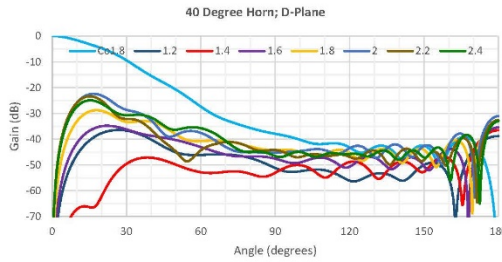
Figure 18. Simulated Copolar (H, E-planes), Crosspolar (D-plane) Patterns of ACFH for $\theta_s=46^\circ$.



(a) Copol, H-plane

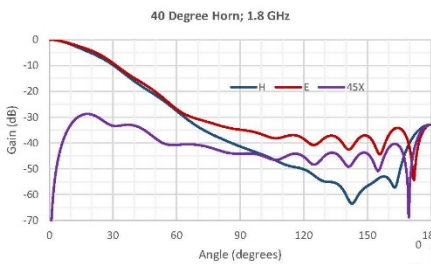


(b) Copol, E-plane

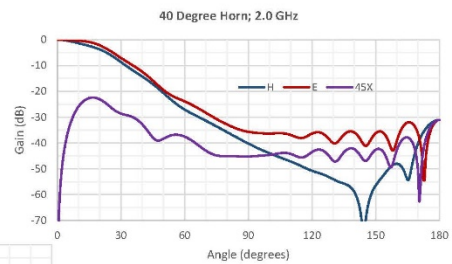


(c) Crosspol, D-plane

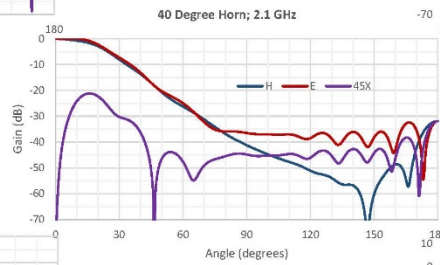
Figure 19. Simulated Copolar, Crosspolar Patterns of ACFH for $\theta_s=41^\circ$.



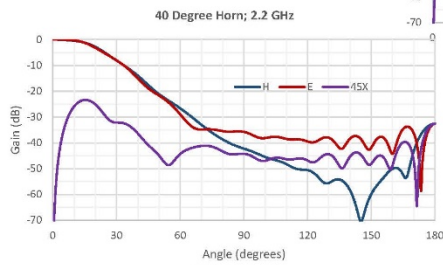
(a) 1.8 GHz



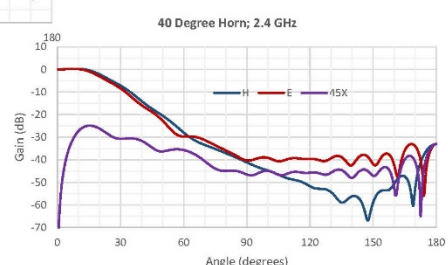
(b) 2.0 GHz



(c) 2.1 GHz



(d) 2.2 GHz



(e) 2.4 GHz

Figure 20. Simulated Copolar (H, E-planes), Crosspolar (D-plane) Patterns of ACFH for $\theta_s=41^\circ$.

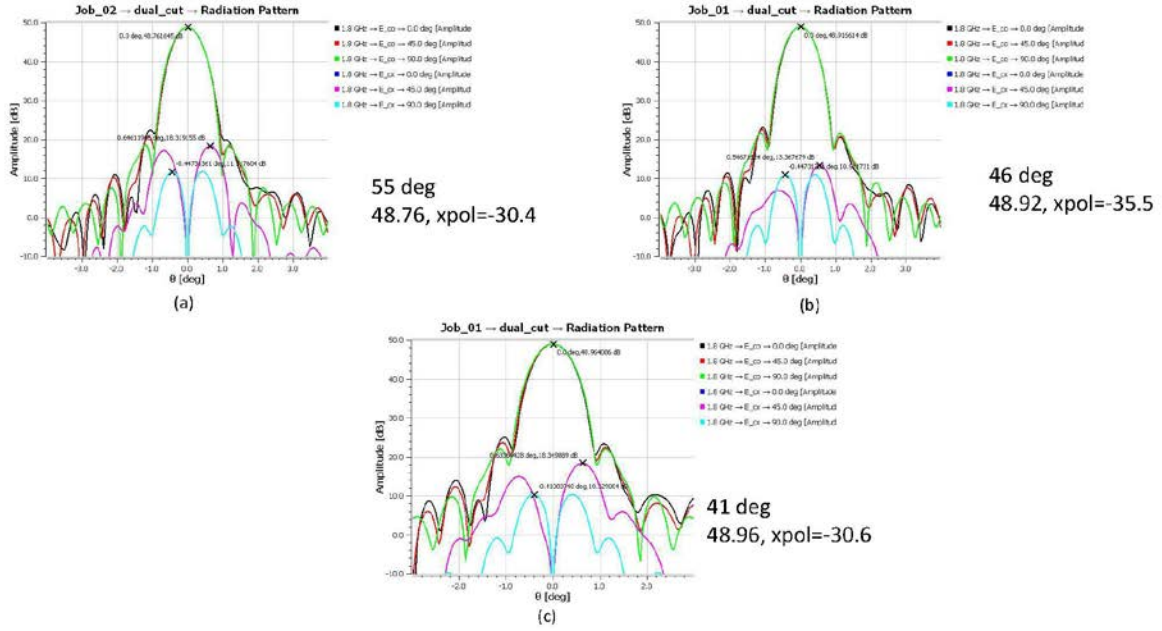


Figure 21. Antenna Beam at 1.8 GHz with ACFH (a) $\theta_s=55^\circ$, (b) $\theta_s=46^\circ$, (c) $\theta_s=41^\circ$.

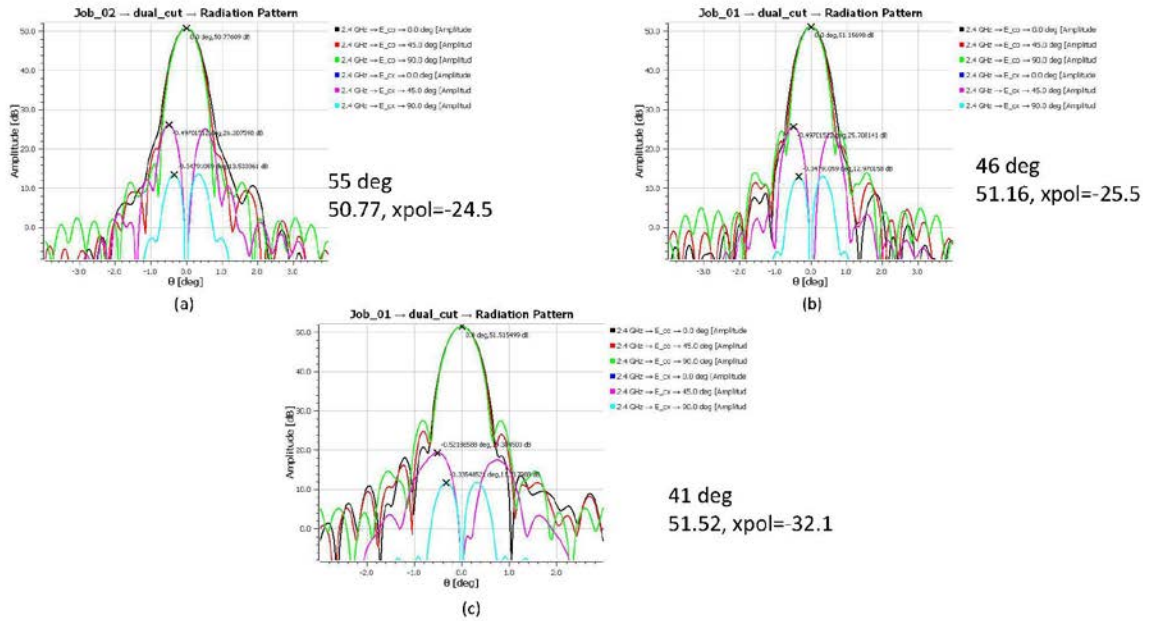


Figure 22. Antenna Beam at 2.4 GHz with ACFH (a) $\theta_s=55^\circ$, (b) $\theta_s=46^\circ$, (c) $\theta_s=41^\circ$.

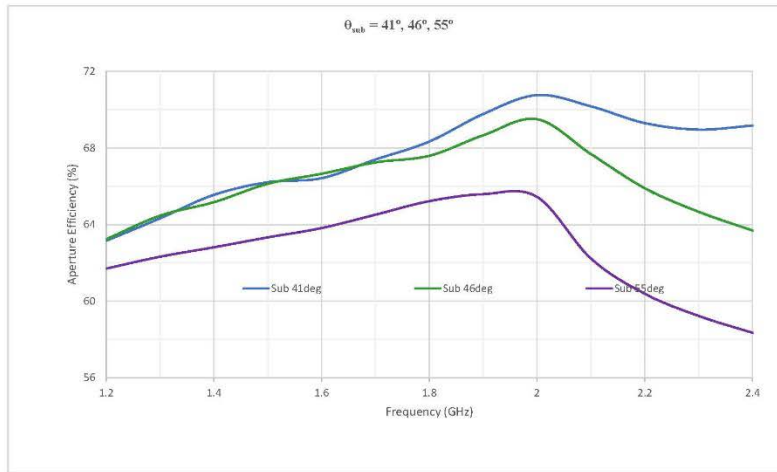


Figure 23. Aperture Efficiency (1.2-2.4 GHz) for $\theta_s=55^\circ$, $\theta_s=46^\circ$, $\theta_s=41^\circ$.

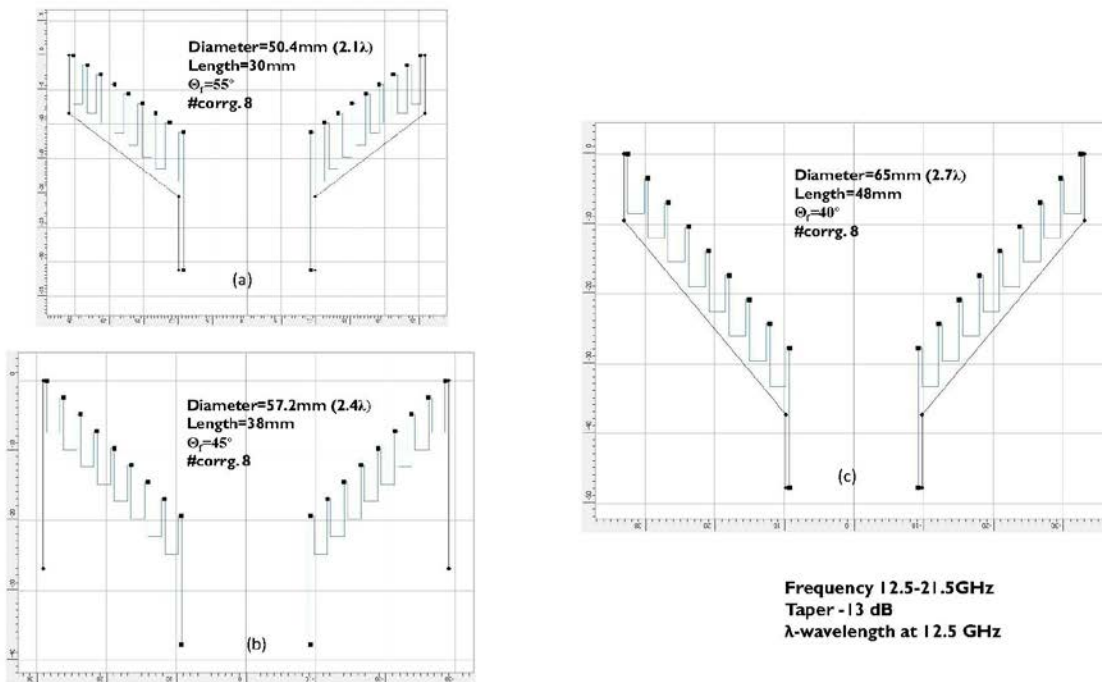


Figure 24. Axially Corrugated Feed Horn (12.5 – 21.5 GHz) for (a) $\theta_s=55^\circ$, (b) $\theta_s=46^\circ$, (c) $\theta_s=41^\circ$.

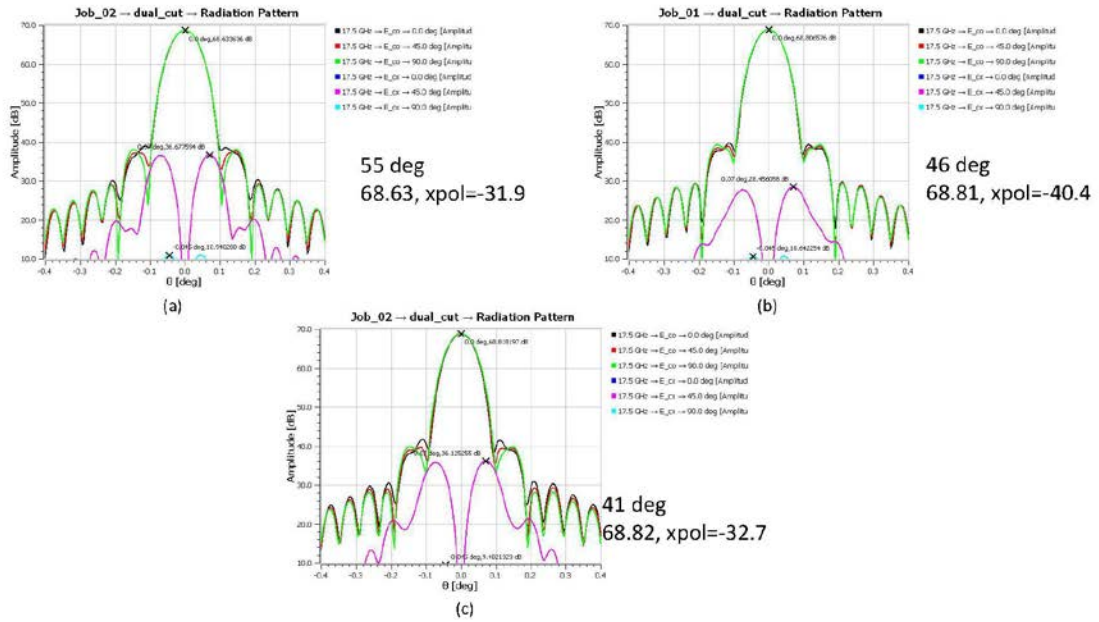


Figure 25. Antenna Beam at 17.5 GHz with ACFH (a) $\theta_s=55^\circ$, (b) $\theta_s=46^\circ$, (c) $\theta_s=41^\circ$.

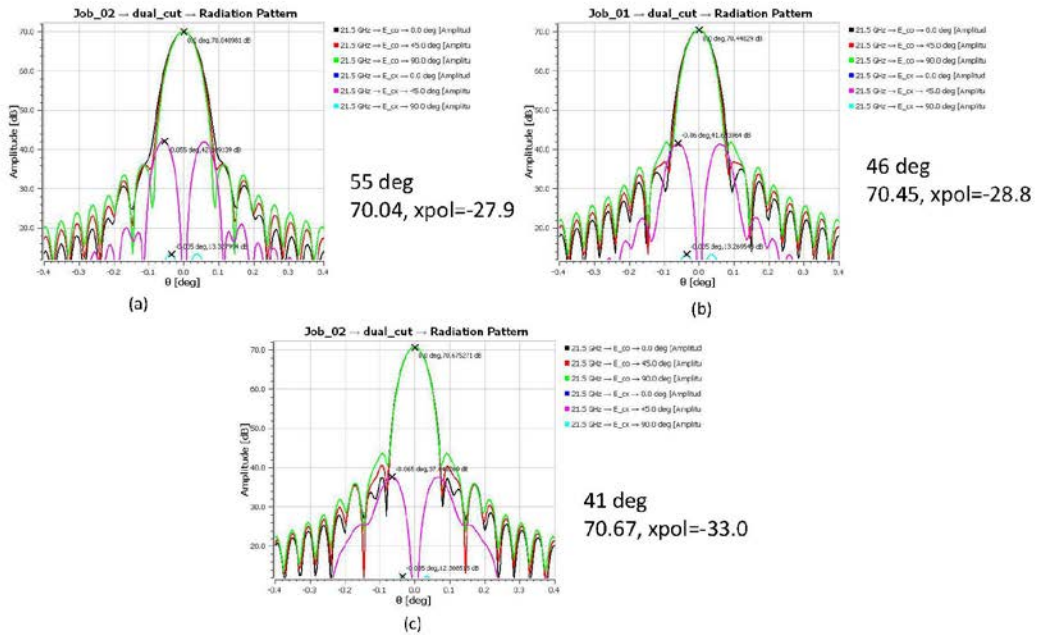


Figure 26. Antenna Beam at 21.5 GHz with ACFH (a) $\theta_s=55^\circ$, (b) $\theta_s=46^\circ$, (c) $\theta_s=41^\circ$.

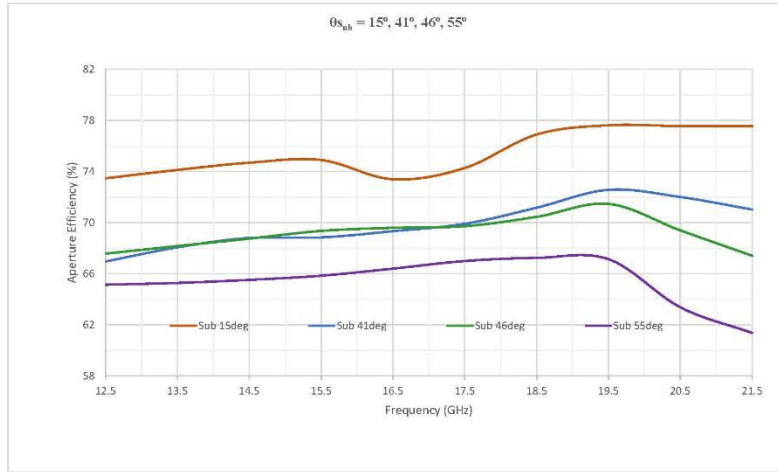


Figure 27. Aperture Efficiency (12.5-21.5 GHz) for $\theta_s=55^\circ$, $\theta_s=46^\circ$, $\theta_s=41^\circ$.

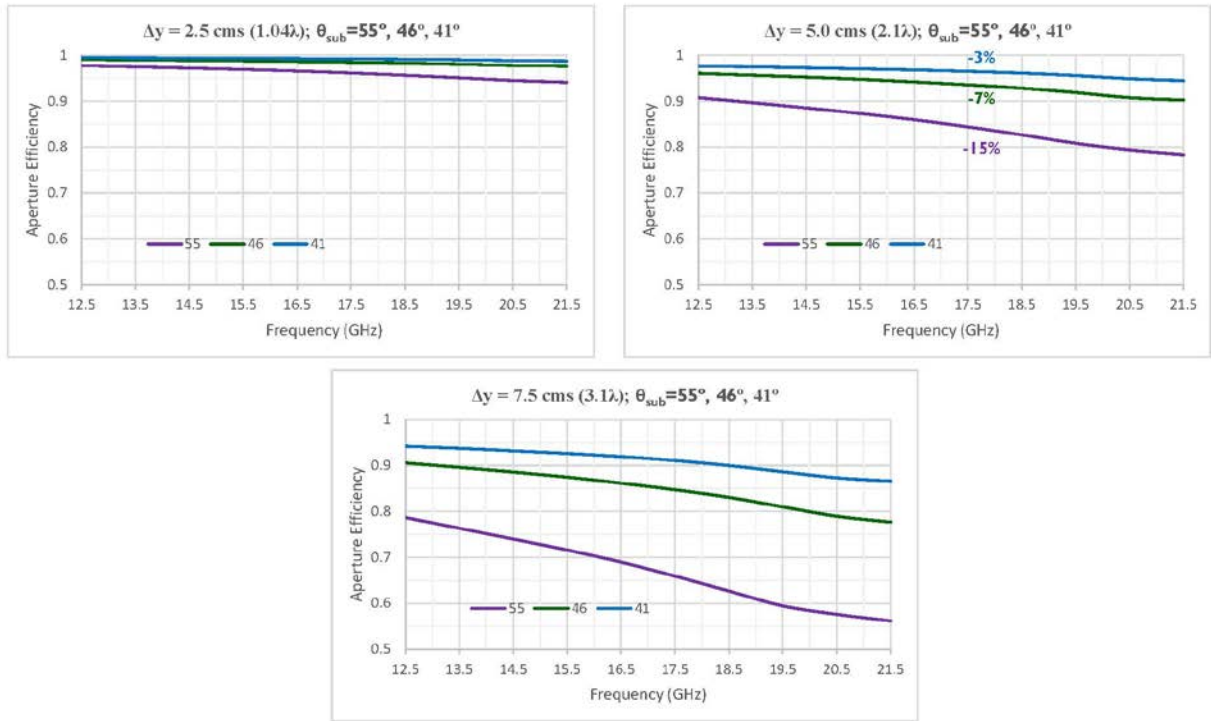


Figure 28. Scanning Performance (12.5-21.5 GHz) for $\theta_s=55^\circ$, $\theta_s=46^\circ$, $\theta_s=41^\circ$.